



CHORUS

This is the accepted manuscript made available via CHORUS. The article has been published as:

Determination of the optical bandgap of the Bernal and rhombohedral boron nitride polymorphs

Adrien Rousseau, Matthieu Moret, Pierre Valvin, Wilfried Desrat, Jiahan Li, Eli Janzen, Lianjie Xue, James H. Edgar, Guillaume Cassabois, and Bernard Gil

Phys. Rev. Materials **5**, 064602 — Published 16 June 2021

DOI: [10.1103/PhysRevMaterials.5.064602](https://doi.org/10.1103/PhysRevMaterials.5.064602)

The Determination of the Optical Bandgap of the Bernal and Rhombohedral Boron Nitride Polymorphs

Adrien Rousseau^a, Matthieu Moret^a, Pierre Valvin^a, Wilfried Desrat^a, Jiahua Li^b, Eli Janzen^b,
Lianjie Xue^b, James H. Edgar^b Guillaume Cassabois^a and Bernard Gil^{a*}

a : Laboratoire Charles Coulomb (L2C), UMR 5221 CNRS-Université de Montpellier, F-34095 Montpellier, France

b : Tim Taylor Department of Chemical Engineering, Kansas State University, Manhattan, Kansas 66506, USA

** corresponding author Bernard.gil@umontpellier.fr*

ABSTRACT

We report a study of polymorphic boron nitride samples. We interpret the photoluminescence line at 6.032 ± 0.005 eV, that can be recorded at 8K in sp^2 -bonded boron nitride, as being the signature of the excitonic fundamental bandgap of the Bernal (or graphitic) boron nitride polymorph (bBN). This is determined by advanced photoluminescence measurements combined with x-ray characterizations on pure hexagonal boron nitride (hBN) and on polymorphic crystal samples, later compared with the theoretical predictions of Lorenzo Sponza, et al., Physical Review B **98**, 125206 (2018). The overall picture is consistent with a direct excitonic fundamental bandgap of the Bernal (or graphitic) polymorph of boron nitride. This value $dX_b = 6.032 \pm 0.005$ eV is higher than the indirect bandgap of hBN ($iX_h = 5.955 \pm 0.005$ eV).

I. INTRODUCTION

Boron nitride (BN) was synthesized as early as 1842 by chemist W.H. Balmain¹ in the form of a white powder. Its individual microcrystals are typically as flat thin round or hexagonal platelets. About one century later, it was established that several different BN phases or polymorphs can co-exist, depending on their synthesis protocols and chemical environmental conditions²⁻⁶. There are specific stable periodic crystalline phases that were identified in the thermodynamic pressure-temperature phase diagram of BN, as represented by figure 2 of reference 7 among which are either sp^3 -type or sp^2 -type bondings. Atoms in the contexts of the *non-centro-symmetric* $F\bar{4}3m$ (T_d^2) cubic phase (cBN, borazone) and the *non-centro-symmetric* $P6_3mc$ (C_{6v}^4) wurtzite phase (wBN) are “fourfold”-coordinated, with sp^3 type bonding. There are many phases based on sp^2 bonding, among which *centro-symmetric*, hexagonal BN or white graphite² $P6_3/mmc$ (D_{6h}^4) (hBN) is the most intensively studied, the *non-centro-symmetric*, rhombohedral BN $R3m$ (C_{3v}^5) (rBN) is occasionally reported, and the Bernal polymorph $P\bar{6}2m$ (D_{3h}^3) (bBN or gBN) is least studied. The latter earns its name due to the similarity to the stacking sequence found in graphite. The hardness of the crystals under these various phases are very different^{8,9}. Single-wall and multi-wall boron nitride nanotubes also exist¹⁰

Other phases, namely pyrolytic (pBN)¹¹ and turbostratic (tBN) boron nitride phases are generally deposited by the reaction of ammonia and a boron halide under high temperature and high vacuum conditions and they are formally analogous to the turbostratic graphite¹². They can be defined as trigonal B_3N_3 hexagon layers stacked roughly parallel to each other, sometimes bent, with a random rotation and translation about the layer normal¹³. Crystallographic and X-ray diffraction measurements indicate the presence of some two-dimensional ordering of atoms. For these phases, the c -lattice constant is larger than the value (0.333 nm) for the AA' (hBN) three-dimensional ordered stacking. The value of c is significantly increased in disordered crystals, reaching 0.356 nm in pure tBN. The average stack height L_c of a parallel layer group consists of four to five layers while the average layer diameter L_a is much longer¹³. The structures of pBN and tBN are similar. Their difference is more or less of the order of semantics, most likely hidden under different degrees of the coherence length of the stack height L_c and the disorder of the orientational twist. The importance of all chemical actors contributing to the growth of the different partner phases at different steps of structural transitions between atomic ensembles with various degrees of disorder are reported in 14, as well as the interpretation of the global shape of the X-ray patterns and the values of c (measured as sitting in the 0.33-0.356 nm range) in terms of multi-phase

mixings¹⁵. The thermal transformation of tBN into the stable, hexagonal ordered layer lattice structure can be triggered by using ad-hoc heat treatments¹⁶.

Recently, interesting physical properties of tBN have been reported among which are its high thermal conductivity¹⁷, chemical stability at high temperature¹⁸, and negative electron affinity¹⁹, as well as the possibility to use it as a precursor for the growth of high quality hBN. They have boosted it out of the laboratories of basic science, into the application arena²⁰ at the same time than hBN was grown under the form of single crystals with millimetric sizes showing laser operation at 215 nm at room temperature^{21,22}

hBN is subject of an abundant literature and a full review is not in the scope here. Briefly, modern epitaxial growth methods can grow rather high quality hBN films on a large variety of different substrates, including metals with high melting temperatures²³. Its integration as a sacrificial layer for cleaving an LED from its substrate is well established²⁴, as is the large scale hetero-epitaxy of hBN with Transition-Metal Di-chalcogenides (TMDs)²⁵. Little attention has been dedicated so far to the epitaxial growth of rBN²⁶⁻²⁹. This polymorph results from a strong interaction with the growth substrate. Determining whether the deposited layer is the hBN or rBN polymorph is challenging, but it can be done by carefully interpreting accurate X-ray measurements (see figure 1 of reference 14, table II of reference 29, figure 6 of 30). Even fewer studies have been dedicated to the Bernal polymorph.

The purpose of this paper is to propose an interpretation of PL measurements at 8K as being the signature of the fundamental excitonic bandgap of Bernal or graphitic boron nitride stacking (bBN) which is direct in reciprocal space with a value of $dX_b = 6.032 \pm 0.005$ eV. This is higher than the indirect bandgap of hBN ($iX_h = 5.955 \pm 0.005$ eV). To ensure the universality of our result we studied samples of pure hBN, and mixed phase crystals hBN/rBN/bBN in the hBN-rich composition range grown using different approaches.

The large number of hBN/rBN/bBN interfaces in our samples caused us to anticipate that measuring a consolidated value for the excitonic bandgaps of either bBN or rBN would not be easy, as the understanding of the origin of the PL of hBN has been cumbersome. It is dominated by defects with a broad band at 5.47 eV, and the indirect excitons that probe the indirect nature of the bandgap generally give weaker features at high energy. The strong and efficient interactions of excitons with phonons complicate the understanding of the light-matter interaction processes^{31,32}. However, the indirect nature of the bandgap could be unambiguously demonstrated³²⁻³⁴ after a series of high-resolution polarized PL experiments that revealed the well-marked phonon-assisted recombinations and the weak and tiny signature of the forbidden indirect exciton iX at 5.955 eV at 4K^{32,33}.

This value is lower by 170 meV than the value of the direct bandgap obtained by a reflectivity experiment at 8K: $dX_h = 6.125 \text{ eV}$ ³⁵. This value for the band gap is supported by the simultaneous complementary observation of phonon assisted structures forming, at lower energy a perfect mirror symmetry between phonon-absorption-assisted transitions (seen in reflectance) and phonon-emission-assisted transitions (seen in luminescence) around the iX_h energy position, both in energy and intensity³⁵. The large energy splittings between 6.032 eV and these two values (5.955 eV and 6.125 eV) related to the hBN phase rules out any misleading contributions of inhomogeneous broadening effects. In addition, the value of the bandgap of the BN monolayer measured by PL is $dX_{ml} = 6.080 \text{ eV}$ ³⁶, therefore an artifact measurement on a delaminated monolayer piece of hBN is also ruled out.

II. SAMPLES

The samples we study here are (001- oriented flakes that were grown by precipitation from a metal solution which led to very high quality crystals. hBN crystals have been grown while testing a variety of solvents for their efficacy to produce high quality large hBN flakes (pure Fe²⁵ and mixtures of Fe+Cr^{37,38}), or carbon-doped hBN (Ni+Cr+C^{39,40,41}). The solution is saturated with boron and nitrogen, then the BN is formed by precipitation during slow cooling (0.5 to 4°C/h) from 1550°C for 25 to 50°C.

Three types of samples were prepared.

- The standard growth used pure Fe as the solvent and hot pressed boron nitride as the boron source. The growth occurred in a H₂ + N₂ forming gas. *This protocol* permits to obtain very high quality monophase hBN crystals with large areas of defect-free material that micro-PL indicates to be *almost* free from impurities. This sample is labelled “Fe”, and the details of its growth are detailed in 25.
- A series of hBN were grown using iron plus vanadium the latter element added to study its potential to enhance nitrogen solubility of the solution for producing thicker crystals. Here the photoluminescence and x-ray diffraction characterization of a BN crystal grown from a 95% Fe+5%V solvent mixture are reported. For this sample, elemental boron with the natural distribution of boron isotopes was the boron source. The growth also occurred in a H₂ + N₂ forming gas. This sample is labelled “Fe+V.”
- The third sample was grown with intentionally added carbon. The solvent was Ni+Cr, and the boron source was a mixture of 20% ¹⁰B and 80% ¹¹B. A CO + N₂ atmosphere was employed. The CO was used instead of hydrogen, to avoid etching of the carbon. This sample is labelled “C+Ni+Cr.”

III. X-RAY MEASUREMENTS

We have plotted in figure 1 the theoretical relative intensities of the different diffraction peaks of BN powders, in the rBN (or ABC stacking), bBN (or AB stacking), hBN (or AA' stacking) and in the thermodynamically less stable hexagonal form (AA stacking) against the diffraction angle 2θ . The x-ray source is copper. The Miller indices are given for all these polymorphs in the hexagonal representation in table I. Obviously many diffraction angles are common to all the polymorphs and the distinction between rBN, hBN and bBN phases in (001) oriented crystals will not be possible as the stacked planes diffract at the same angles: $\sim 27^\circ$, $\sim 55^\circ$ and $\sim 88^\circ$. Interestingly, diffraction on slightly disoriented samples allows detection of complementary peaks indicated using diamonds for rBN and hearts for hBN and bBN at specific phase-discriminative angles in figure 1. The likely coexistence of the hBN and bBN polymorphs in real multilayer samples makes their distinction extremely subtle.

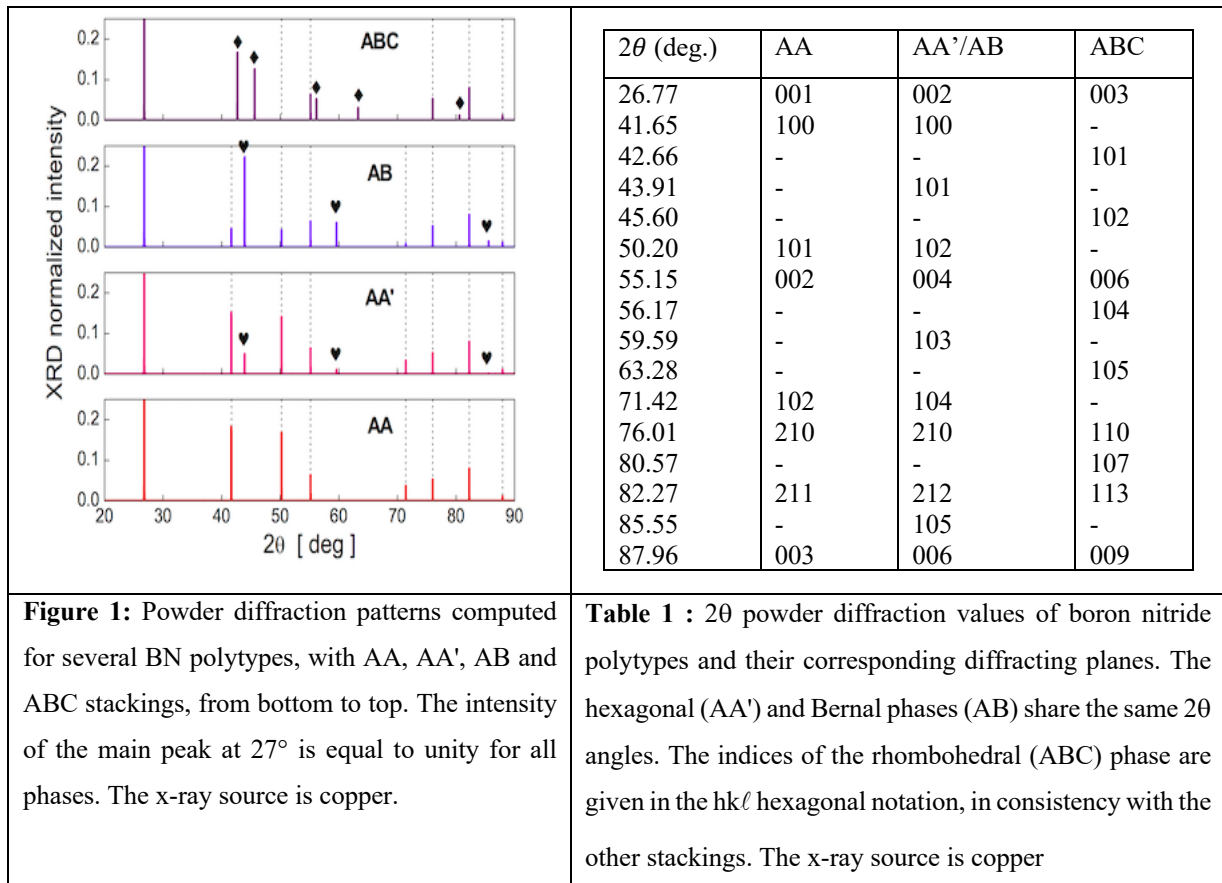


Figure 2 represents a series of X-ray diffraction spectra which were recorded at room temperature, in the Bragg-Brentano configuration using a Bruker D8DISCOVER diffractometer with a VÅntec linear detector. To increase the detectivity, we have used a simple Göbel mirror resulting in a non-monochromatic primary beam: $(Cu(K\alpha_1+K\alpha_2))$ with some traces of $Cu(K\beta)$ and $W(LA1)$. According to references 14, 28, 29 and 30, figure I and table I,

the complex features overlapping in the 40° - 45° region for sample C+Ni+Cr (plot in green) are the evidence of the coexistence of hBN and rBN. They are not observed for Fe+V (red plot) or Fe (blue plot). In case of purely oriented (001) films and in the θ - 2θ condition, as alluded to earlier in this paper, only (002), (004) and (006) diffractions are expected at $\sim 27^{\circ}$; $\sim 55^{\circ}$; and $\sim 88^{\circ}$ angles respectively. Although the samples have been carefully removed from the eutectic solidified they have been slightly folded and this leads to the additional diffraction features for instance of the [hk0] type, thanks to the sensitivity of our experiment.

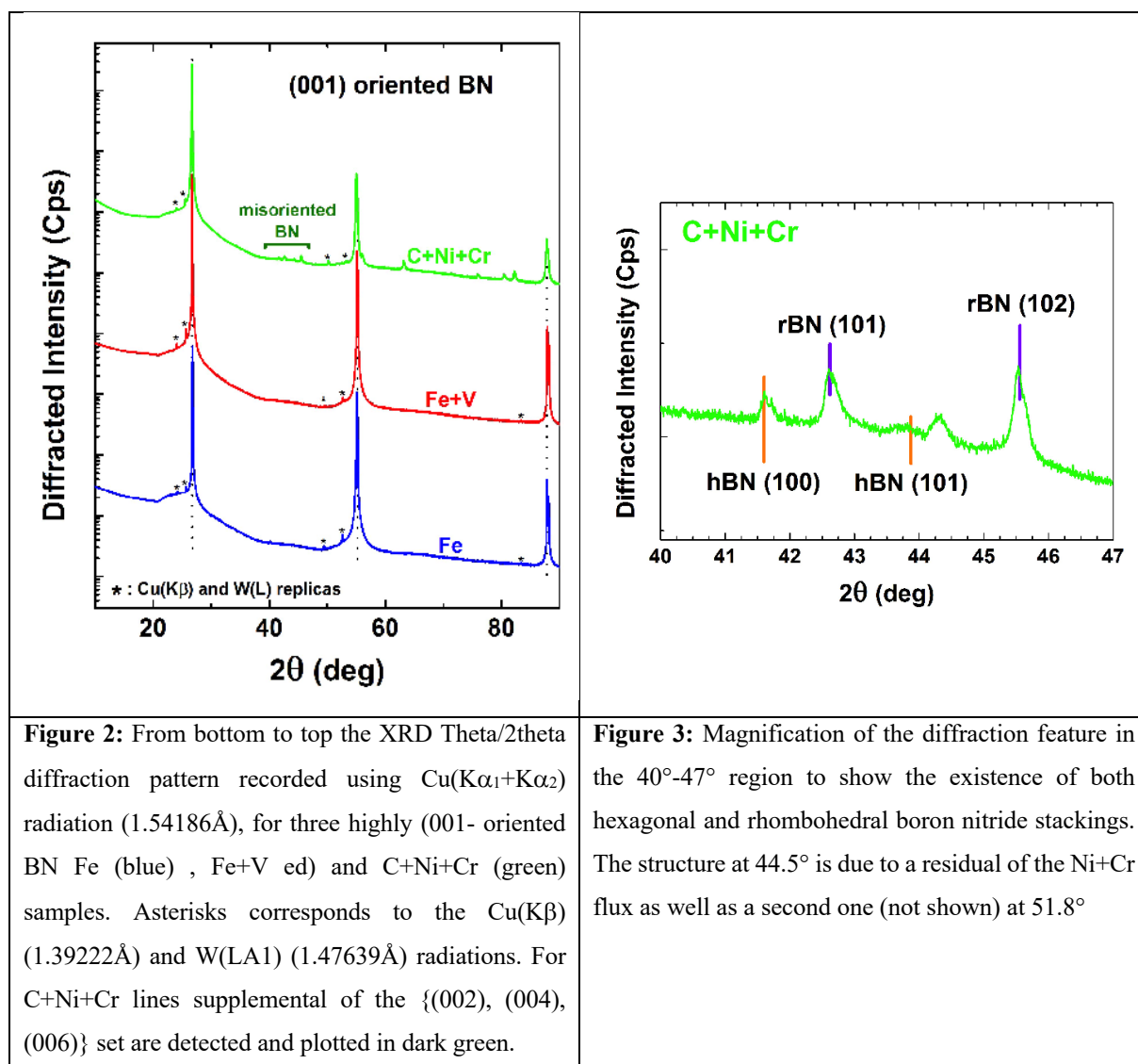


Figure 2: From bottom to top the XRD Theta/2theta diffraction pattern recorded using Cu($K\alpha_1+K\alpha_2$) radiation (1.54186\AA), for three highly (001)- oriented BN Fe (blue) , Fe+V (red) and C+Ni+Cr (green) samples. Asterisks corresponds to the Cu($K\beta$) (1.39222\AA) and W(LA1) (1.47639\AA) radiations. For C+Ni+Cr lines supplemental of the $\{(002), (004), (006)\}$ set are detected and plotted in dark green.

Figure 3: Magnification of the diffraction feature in the 40° - 47° region to show the existence of both hexagonal and rhombohedral boron nitride stackings. The structure at 44.5° is due to a residual of the Ni+Cr flux as well as a second one (not shown) at 51.8°

The departure from perfect Bragg-Brentano geometry and/or inclusions of small amounts of polymorphism can both lead to supplementary peaks⁴². This is illustrated in figure 3 which displays a magnification of the 40° - 47° region for sample C+Ni+Cr. There are obviously disorientated parts in the hBN crystal, as indicated on the one hand by the recording of the (100), (101) and (102) diffraction peak of hBN expected near 41.66° , 43.91° and 50.20° respectively AND rhombohedral inclusions as evidenced by the recording of the (101) , (102)

diffractions peaks of the rBN near 42.66° and 45.60° respectively, at angles fitting with the prescriptions in table I and in table II of reference 29. This sample is a multi-phase crystal. There is no diffraction peak at 26.30° that would have proven the presence of tBN (figure 4 of 27). Rocking curves are flat for the powder and for sample C +Ni +Cr , indicating a distribution of orientations. Rocking curves of Fe and Fe+V (not shown) are composite, made of distributed series of sharp peaks, a shape typical of high quality layered compounds 38.

IV.PHOTOLUMINESCENCE

The PL is measured at liquid Helium temperatures ($T=8$ K) in a closed-cycle cryostat with an excitation energy of 6.35 eV (195 nm) that is greater than the bandgap of BN. The optical setup consists mainly of a cw mode-locked Ti:Sa laser that produces an output power of 30 uW, a Czerny-Turner monochromator equipped with a 1800 grooves/mm grating and a back-illuminated CCD camera for the detection. The lateral size of the laser spot at the sample surface is about 50 μm .

In figure 4 are gathered some low temperature PL features collected in the 5-6.1 eV range. The spectra from the bottom to the top correspond to: *i*) a pure hBN crystal grown using $^{\text{nat}}\text{B}$, N_2 and the Fe flux (Fe blue) , *ii*) hBN, grown again using $^{\text{nat}}\text{B}$, N_2 and the Fe+V flux (Fe+V red) , *iii*) the PL of the sample grown with carbon C+Ni+Cr green).

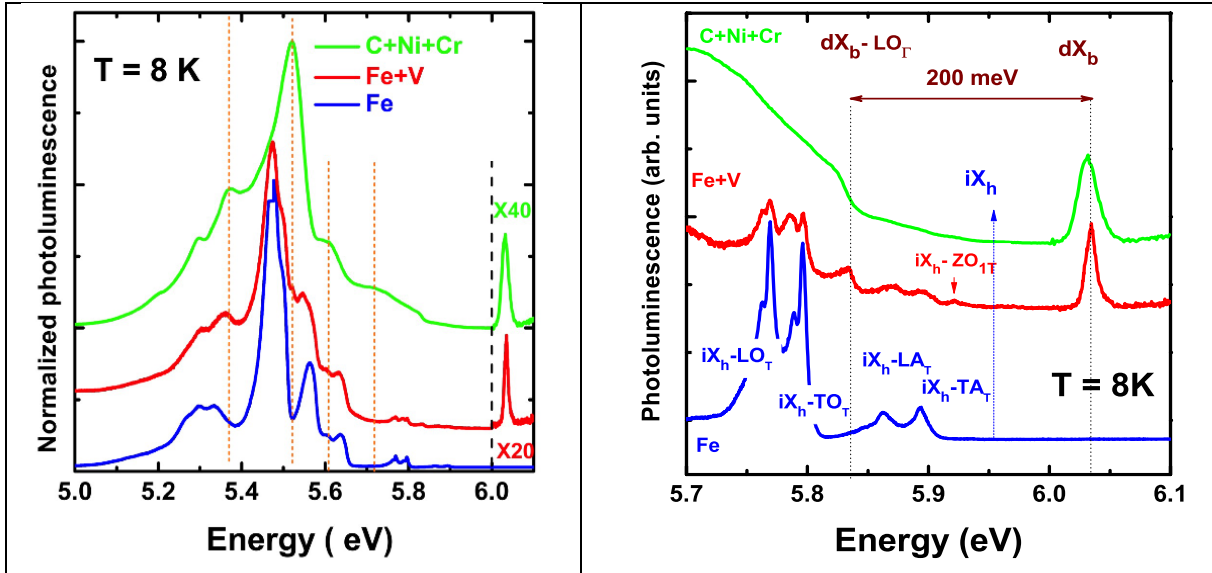


Figure 4:The 8K macro PL spectra in the 5 eV to 6.1 eV range of several samples showing the phonon-assisted transitions typical of hBN (blue spectrum), mixed with the undulations linked to rBN inclusions overlapping with impurities (green and red spectra) as well as signature of the direct bandgap of bBN, dX_b at 6.032 eV. We tentatively identify the 5.72 eV band in C+Ni+Cr as the unresolved analogue of the $iX_h-(LO_T + TO_T)$. Dashed orange lines are guides for the eyes.

Figure 5: Enlarged view of the 8K macro PL spectra in the 5.7eV to 6.1 eV range that reveals the signature of the direct bandgap of bBN at 6.032 eV as well as its 200 meV phonon-assisted replica (green and red spectra). In blue the macro PL of a high purity hBN crystal. Transitions are labelled according to the convention in the literature. State T sits at the middle of the ΓK direction in the Brillouin zone of hBN.

The most intriguing feature is the sharp transition noted dX_b at 6.032 ± 0.005 eV in samples Fe+V and C+Ni+Cr, and the weak structure at ~ 200 meV below, that is more clearly seen in the magnification of the 5.7eV-6.1 eV region in figure 5, which is broader for C+Ni+Cr. This feature occurs at an energy of 5.83 eV, a value intermediate between the energy of the iX_h - LA_T and iX_h - TO_T phonon-assisted transitions of hBN. In addition, we disregard an overtone of the one phonon iX_h - ZO_{1T} assisted transition recorded at 5.93 eV with a complementary ZO_{1T} phonon at the middle (along the ΓK direction) of the Brillouin zone, thanks to intensity arguments *and because* we have not recorded it before when studying accurately the contributions of phonon symmetries in hBN³³. *In sample C+Ni+Cr, the high energy side of this line is well resolved, like in Fe+V. The contribution of the many more defects to the global PL spectrum of this sample overlaps with its low energy wing, thus unfortunately preventing us from clearly resolving it.* From all these experimental arguments and from the lack of such structure in our test sample Fe, we attribute this line as a phonon replica of the 6.032 eV line. The 200 meV splitting is energy- and symmetry-compatible with an *LO phonon at Γ* which replicates efficiently thanks to the Frölich interaction process. *The variation of the intensity and energy of the dX_b line slightly varies over the samples and we safely frame its average value as 6.032 ± 0.005 eV with a similar uncertainty as in hBN.*

Since the transition dX_b at 6.032 ± 0.005 eV transition cannot be recorded in high quality hBN, it is the signature of a deviation from perfect AA' stacking. As we discuss in the last part of this paper, the sharp transition dX_b at 6.032 ± 0.005 eV and the mechanism of replication with an LO_T phonon at zone-centre indicate the existence of bBN inclusions with a *direct bandgap*. Here the bBN inclusions are embedded in an hBN material with an indirect bandgap giving PL with many phonon-assisted transitions involving phonons at the T point of the Brillouin zone.

V.DISCUSSION

Although the existence of rBN inclusions was revealed by X-ray diffraction experiments, bBN was not detected. At this stage, the question of the PL signatures of tBN and rBN remain opened. Back to the PL spectra, they globally display the same shapes, with similar kinds of broad undulations over the three samples. Some of these undulations are sometimes spectrally shifted (C+Ni+Cr) with respect to the ones traditionally recorded in hBN when the dX_b transition at 6.032 eV is not recorded (Fe). This indicates the evidence of a similarity among the differences that have been quoted by theoretical studies of the optical properties of hBN and rBN⁴³. In the specific case of sample Fe+V two interpenetrating series of undulations are detected as seen in figure 4, the hBN-related series being far from the dominating one. We thus

deduce that the optical signatures of hBN and rBN obtained from a simple PL experiment occur at different energies but overlap in a large energy range. *We believe that the similarity of the shape of defect-related PL bands in hBN and rBN from bona fide infer for an indirect band structure for rBN, in contrast to bBN for which the bandgap is direct in reciprocal space.* To consolidate this statement, we recall the PL of hBN, which is an unusual semiconductor in terms of light-matter interaction, as both extrema of the fundamental valence and conduction bands are sitting at different edges of the Brillouin zone⁴⁴⁻⁴⁷. The singularity of this material, compared to other indirect band gap materials resides in its specific indirect fundamental bandgap with the minimum of the conduction band sitting at the **M** point of the Brillouin zone, and the maximum of the valence band sitting in the close neighbourhood of **K**. The PL that can be recorded in the ultraviolet is based on spatially delocalized⁴⁸ one-phonon-assisted recombinations (phonons with an **MK** wavevector that translational symmetry brings equivalent to $\frac{\Gamma K}{2}$, that is to say a wave vector at the middle of the Brillouin zone along the ΓK direction) in the 5.7 to 5.9 eV range^{31,32}. The energies of these transitions shift in samples monoisotopic pure in boron³³ as the phonon energies change when ¹⁰B or ¹¹B are used instead of the natural boron (^{nat}B is made of 20% ¹⁰B and of 80% ¹¹B). In very high-quality crystals, the low energy wings of the PL features are structured thanks to a complementary Raman scattering process involving the low frequency (E_{2g}) normal vibration mode⁴⁷. Starting from 5.6 eV down to 5.3 eV or less transitions localized to *surface layer foldings* with ad-hoc sizes and orientation exist⁴⁸. These localized emissions form a ladder of features and they enhance the overtone featuring of the higher energy phonon assisted transitions^{49,50}. They are neither observed in micro cathodoluminescence⁵¹ nor in micro-PL experiments⁵² recorded in defect-free regions of hBN. They are the signature of complementary intervalley scattering assisted by TO(**K-K'**) phonon modes⁵⁰. The surface layer foldings permit to simultaneously fulfill the requirements of the different conservation laws and offer the density of state required to bring the radiative recombination rate of Fermi's golden rule to substantial values that permits to extract radiative recombination from the experimental parasitic noise. Some contributions of recombination lines namely D₂ and D₆ attributed to defects^{50,53} and un-identified impurities⁵² are also detected in this energy range, as well as more sophisticated many-impurity localization centres^{54,55}. At energies below 4 eV down to 1.5 eV roughly, are a series of more or less broad transitions attributed to still unknown impurities, to boron-vacancy complexes. All of them operate as single photons emitters, which indicates that hBN is a promising crystal for quantum technologies²³. The global shape of the full PL spectrum revealing the strong exciton-phonon

coupling^{31,56} has been recently computed theoretically^{57,58} as an evidence of the degree of maturity reached in the understanding of the optical properties of hBN.

The broad undulating bands in all samples correspond to radiation by phonon-assisted carrier recombination not to carriers localized to defects. The whole series of these phonon-assisted recombinations cascading from 5.955 eV down to 5.62 eV in hBN requires large areas of material, and features are observed at lower energies in defective areas. We believe that the crystalline quality of rBN as well as the density of defect prevents us from detecting similar effect here as the contributions of the different phases overlap (*by the way, this statement also holds regarding the bBN inclusions*) with the hBN related features. From this, we derive the global energy shifts and PL shapes. Regarding the relative proportions of the different polymorphs, it is not easy to evaluate quantitatively.

There have been a few reports regarding the electronic structure of alternative stacking like for instance a Bernal (graphite) stacking or others^{39,59-66}. Sponza *et al.*⁴³ have predicted a direct band gap for bBN, and indirect ones for hBN and rBN with *bBN having the highest value of the three and rBN the smallest*. Our paper offers some new experimental confirmation of this, in terms of PL energies. The observation of PL line dX_b (even tiny) at 6.032 ± 0.005 eV supports the existence of bBN inclusions in the hBN. The replica red-shifted by 200 meV, can only be the energy of the so-called LO_3 phonon branch at zone center⁵⁷. Because this phonon does not carry any wavevector and does not change the momentum balance in the recombination process, a replica involving this phonon either simply reproduces a sharp excitonic line in the case the exciton is direct, or contributes to the formation of a series of lines that are red-shifted by 200 meV with respect to the main series of phonon-assisted lines in the case the exciton is indirect. In contrast to hBN, we do not observe here a complex series of lines neither at ~ 6.03 eV nor at ~ 5.83 eV, which strongly supports the direct nature of the recombination process giving rise to the PL signal at 6.03 eV in particularly good agreement with the accurate calculation of ref. 44. Still in the framework of Sponza *et al.*⁴³, which predict similarities between the phonon-assisted transitions and defect-related PL bands of rBN and hBN, and from the broad PL bands in Sample Ni+Cr+C, we are inclined to tentatively suggest an indirect fundamental band structure for rBN. Unfortunately, this overlap of emission from different polymorphs prevents us from detecting the analogue of the indirect exciton iX in hBN which could not be unambiguously evidenced in our samples, in the range of energy proposed by Sponza *et al.*⁴³ (about 5.4 eV) a pure rBN crystal should be required for that, which does not exist to date. This is mandatory as all the phonon modes being both Infra-Red and Raman active, the set of phonon-assisted transitions is probably more documented than in the (already) complicated hBN case. Note that

there has been a recent report for the optical value of the bandgap of tBN: 5.82 eV at room temperature, a value deduced from a Tauc plot analysis of transmission experiments⁶⁷. The next question that comes to our mind should be treated by theorists as it is : how are interconnected the band line-ups at the rBN-hBN interface, the bBN-hBN interface, the rBN-bBN interface: are they type I or type II, are they both? Then, based on the weak cross-talking of carriers photo-created in both phases, and the apparent possibility to tune the density of rBN inclusions by growth conditions, it would become very tempting to envision extending the spectral range of single photon emission operation actually limited to 4.1 eV⁶⁸ up to the Deep Ultra Violet, at least at low temperature.

VI.CONCLUSION

We have studied the optical signature at 8K for bulk boron nitride crystals that X-Ray indicate to be “pure” hexagonal boron nitride (hBN), and sometimes multiphase-samples consisting of dominating hBN contaminated by inclusions of rhombohedral boron nitride (rBN). Based on our preceding observation of an indirect excitonic band gap iX_h at 5.955 eV, and a direct one dX_h at 6.125 eV in hBN, and on the determination of a direct excitonic bandgap at 6.080 eV in a monolayer of boron nitride, we attribute a transition dX_b at 6.032 eV and its phonon replica 200 meV below to the signature of the direct excitonic bandgap of a Bernal stacking (bBN) that is not discriminated by X-ray diffraction from the hBN one in our flake samples.

ACKNOWLEDGEMENTS

We gratefully acknowledge C. L’Henoret for his technical support at the mechanics workshop. This work was financially supported by the network GaNeX (ANR-11-LABX-0014), the BONASPES project (ANR-19-CE30- 0007), the ZEOLIGHT project (ANR-19-CE08-0016) and the Université de Montpellier. Support for BN crystal growth came from the Office of Naval Research, award number N00014-20-1-2474, and the National Science Foundation, award number CMMI #1538127.

REFERENCES

- 1- W. H. Balmain, J. Prak. Chem., vol. **27**, 422(1842).
- 2- R. S. Pease, Acta Cryst., **5**, 356 (1952).
- 3- C. Coulson and R. Taylor, Proc. Phys. Soc. **A65**, 815 (1952).
- 4- R. H. Wentorf, J. Chem. Phys. **26**, 956 (1957).
- 5- H. J. Milledge, E. Nave , and FH. Weller, Nature **184**, 715 (1959).
- 6- L. Zagayansky and G. V. Samsonov, ЖУРНАЛ ПРИЛАДНОЙ ХИМИИ, **25**, 557, (1952), J. Appl. Chem. U.S.S.R. **25**, 629 (1952).
- 7- M.I.Petrescu and M.G. Balint, U.P.B.Sci. Bulletin, Series B, **69**, 35, (2007).

- 8- M.I.Petrescu and M.G. Balint, U.P.B.Sci. Bulletin, Series B, **69**, 43, (2007).
- 9- Alain Polian, Edited by J.H.Edgar, S.Strite, I.Akasaki, H.amano and C.Wetzel, EMIS datareviews series , **23**, 11 (1994) published by INSPEC, the Institution of Electrical Engineers, London
- 10- Nasreen G. Chopra, R. J. Luyken, K. Cherrey, Vincent H. Crespi, Marvin L. Cohen, Steven G. Louie, A. Zettl, Science **269**, 966 (1995).
- 11- A.W. Moore, Journal of Crystal growth, **106**, 6 (1990).
- 12- J. Biscoe and B. E. Warren, Journal of Applied Physics **13**, 364 (1942).
- 13- N.E Thomas Jr., Weston and T.E. O'Connor, Journal of the American Chemical Society **82**, 461 (1962).
- 14- M.G. Balint and M.I.Petrescu, U.P.B.Sci. Bulletin, Series B, **69**, 79, (2007).
- 15- Toshitsugu Matsuda, Naoki Uno, Hiroyuki Nakae, Toshio Hirai, Journal of Materials Science **21**, 649 (1986).
- 16- S. Alkoy, C. Toy, T. Gönül, & A. Tekin, Journal of the European Ceramic Society **17**, 1415–1422 (1997).
- 17- T. Sugino, S. Kawasaki, K. Tanioka, J. Shirafuji, Applied Physics Letters **71**, 2704 (1997).
- 18- K. P. Loh, I. Sakaguchi, M. N. Gamo, S. Tagawa, T. Sugino, T. Ando, Applied Physics Letters **74**, 28 (1999).
- 19- C. Kimura, T. Yamamoto, and T. Sugino, Diamond Related Materials, **10**, 1404 (2001).
- 20- J.Lian, T. Kim, X. Liu, J. Ma, and W. Zheng, , Journal of Physical Chemistry C **113**, 9135 (2009).
- 21- Watanabe, T. Taniguchi, and H. Kanda, Nature Materials, **3**, 3404 (2004).
- 22- K.Watanabe,T.Taniguchi,T.Niiyama,K.Miya,andM.Taniguchi, Nat. Photonics, vol. **3**, 591, (2009).
- 23- Bernard Gil, Guillaume Cassabois, Ramon Cusco, Giorgia Fugallo and Lluís Artús, Nanophotonics **9**, 3483(2020).
- 24- Y. Kobayashi, K. Kumakura, T. Akasaka, and T. Makimoto, Nature **484**, 223 (2012).
- 25- J. Li, J. Wang, X. Zhang, C. Elias, G. Ye, D. Evans, G. Eda, J.M. Redwing, G. Cassabois, B. Gil, P. Valvin, R. He, B. Liu and J.H. Edgar, ACS Nano **15** 7032 (2021).
- 26- Liqiang Xu, Jinhua Zhan, Junqing Hu, Yoshio Bando, Xiaoli Yuan, Takashi Sekiguchi, Masanori Mitone and Dmitri Goldberg, Advanced Materials, **19**, 2141, (2007).
- 27- Mikhail Chubarov, Henrik Pedersen, Hans Högberg, Jens Jensen, and Anne Henry, Crystal Growth Design **12**, 3215 (2012).
- 28- Mikhail Chubarov, Henrik Pedersen, Hans Högberg, Zsolt Czigány, Magnus Garbrecht, and Anne Henry, Chemistry of Materials **27**, 1640 (2015).
- 29- Mikhail Chubarov, Hans Högberg, Anne Henry and Henrik Pedersen, Journal of Vacuum Science and Technology A **36**, 030801 (2018).
- 30- Xiao-Yan Ren, Chun-Xiang Zhao, Chun-Yao Niu, Jia-Qi Wang, Yu Jia, Jun-Hyung Cho, Physics Letters A **380**, 3891 (2016).
- 31- Y. Toyozawa, Prog. Theor. Phys., **20**, 53 (1958).

- 32- Guillaume Cassabois, Pierre Valvin and Bernard Gil, *Nature Photonics* **10** , 262, (2016).
- 33- T. Q. P. Vuong, G. Cassabois, P. Valvin, V. Jacques, A. Van Der Lee, A. Zobelli, K. Watanabe, T. Taniguchi, B. Gil, *2D Mater.* **4** , 011004, (2017).
- 34- T. Q. P. Vuong, S. Liu, A. Van der Lee, R. Cusco, L. Artus, T. Michel, P. Valvin, J. H. Edgar, G. Cassabois, and B. Gil, *Nature Materials* **17**, 152, (2018).
- 35- Kenji Watanabe Takashi Taniguchi, *Physical Review B*, **79**, 193104, (2009), see for instance figure 2(b) and figure 6.
- 36- C. Elias, P. Valvin, T. Pelini, A. Summerfield, C. J. Mellor, T. S. Cheng, L. Eaves, C. T. Foxon, P. H. Beton, S. V. Novikov, B. Gil, and G. Cassabois , *Nature Communications* **10**, 2639 (2019).
- 37- Song Liu, R.He, and Z.Ye, et al., *Crystal Growth Design* , **17**, 4932 (2017).
- 38- J. Li, C. Elias, Z. Ye, D. Evans, S. Liu, R. He, G. Cassabois, B. Gil, P. Valvin, B. Liu and J.H. Edgar, *J. Mater. Chem. C* **8** 9931-9935 (2020).
- 39- T.B. Hoffman, B. Clubine, Y. Zhang, K. Snow, and J.H.Edgar, *J. Cryst. Growth* **393** 114-118 (2014).
- 40- J.H. Edgar, T.B. Hoffman, B. Clubine, M. Currie, X.Z. Du, J.Y. Lin and H.X. Jiang, *J. Cryst. Growth* **403** 110-113 (2014).
- 41- T. Pelini, C. Elias, R. Page, L. Xu, S. Liu, J. Li, J. Edgar, A. Dréau, V. Jacques, P. Valvin, B. Gil, and G. Cassabois , *Phys. Rev. Materials* **3**, 094001 (2019).
- 42- M.G. Balint , M.I. Petrescu , *Diamond & Related Materials* **18**, 1157 (2009).
- 43- Lorenzo Sponza, Hakim Amara, Claudio Attacalite, Sylvain Latil, Thomas Galvani, Fulvio Paleari, Ludger Wirtz, and François Ducastelle, *Physical Review B* **98**, 125206 (2018).
- 44- E. Doni, and G. Pastori Parravicini, *Il Nuovo Cimento B*, vol. **64**, 117 (1969).
- 45- B. Arnaud, S. Lebegue, P. Rabiller, and M. Alouani, *Phys. Rev. Lett.* **96**, 026402 (2006).
- 46- P. Cudazzo, L. Sponza, C. Giorgetti, L. Reining, F. Sottile, and M. Gatti, *Phys. Rev. Lett.*, **116**, 066803 (2016).
- 47- J. Koskelo, G. Fugallo, M. Hakala, M. Gatti, F. Sottile, and P. Cudazzo, *Phys. Rev. B* **95**, 035125 (2017).
- 48- R. Bourrellier, M. Amato, L. H. G. Tizei, et al., *ACS Photonics* **1**, 857 (2014).
- 49- T. Q. P. Vuong, G. Cassabois, P. Valvin, V. Jacques, R. Cusco, L. Artus, B. Gil, *Physical Review B* **95**, 045207 (2017).
- 50- Guillaume Cassabois, Pierre Valvin and Bernard Gil, *Physical Review B* **93**, 035207 (2016).
- 51- Léonard Schué, Lorenzo Sponza, Alexandre Plaud, Hakima Bensalah, Kenji Watanabe, Takashi Taniguchi, François Ducastelle, Annick Loiseau, and Julien Barjon, *Phys. Rev. Lett.* **122**, 067401 (2019).
- 52- Pierre Valvin, Thomas Pelini, Guillaume Cassabois, Alberto Zobelli, Jiahn Li, James H. Edgar, and Bernard Gil, *AIP Advances* **10**, 075025 (2020).
- 53- C.Attacalite, M.Bockstedte, A.Marini, A.Rubio, and L.Wirtz, *Phys. Rev. B* **83**, 144115 (2011).

- 54- Shigefusa F. Chichibu, Youichi Ishikawa, Hiroko Kominami, and Kazuhiko, *Journal of Applied Physics* **123**, 065104 (2018).
- 55- Emi Tsushima, Takuya Tsujimura, and Takashi Uchino, *Appl. Phys. Lett.* **113**, 031903 (2018).
- 56- T. Q. P. Vuong, G. Cassabois, P. Valvin, S. Liu, J. H. Edgar, and B. Gil, *Physical Review B* **95** 201202 (2017).
- 57- F. Paleari, H. P. C. Miranda, A. Molina-Sánchez, and L. Wirtz, *Physical Review Letters* **122**, 187401 (2019).
- 58- E. Cannuccia, B. Monserrat, and C. Attacalite, *Physical Review B* **99**, 081109 (2019).
- 59- T Galvani, F Paleari, H P Miranda, A Molina-Sanchez, L Wirtz, S Latil, H Amara and F Ducastelle, *Phys. Rev. B* **94**, 125303 (2016).
- 60- D Wickramaratne, L Weston and C G Van de Walle , *J. Phys. Chem. C* **122**, 25524 (2018).
- 61- Mengle K and Kioupakis E , *APL Materials*. **7**, 021106 (2019).
- 62- J C G Henriques, G B Ventura, C D M Fernandes and N M R Peres, ,*Journal of Physics: Condensed Matter* **32**, 025304 (2020).
- 63- R. M. Ribeiro, and N. M. R. Peres, *Physical Review B* **83**, 235312 (2011).
- 64- Lei Liu, Y.P.Feng, and Z.X.Shen, *Physical Review B* **68**, 104102 (2003).
- 65- G. Constantinescu, A. Kuc, and T. Heine, *Physical Review Letters* **111**, 036104 (2013).
- 66- S. Matt Gilbert, Thang Pham, Mehmet Dogan, Sehoon Oh, Brian Shevitski, Gabe Schumm, Stanley Liu, Peter Ercius, Shaul Aloni, Marvin L. Cohen, and Alex Zettl, *2D Materials* **6**, 021006 (2019).
- 67- Hisashi Yamada, Naoto Kumagai, Toshikazu Yamada, and Taiki Yamamoto, *Appl. Phys. Lett.* **118**, 112101 (2021).
- 68- R.Bourrellier, , S; Meuret, A. Tararan, O.Stephan, M. Kociak, Mathieu, L.H.G.Tizei, and A. Zobelli , *Nano Letters* **16**, 4317 (2016).

FIGURE CAPTIONS

Figure 1: Powder diffraction patterns computed for several BN polytypes, with AA, AA', AB and ABC stackings, from bottom to top. The intensity of the main peak at 27° is equal to unity for all phases. The x-ray source is copper.

Figure 2: From bottom to top the XRD Theta/2theta diffraction pattern recorded using $\text{Cu}(K\alpha_1+K\alpha_2)$ radiation (1.54186\AA), for three highly (001)- oriented BN Fe (blue) , Fe+V ed) and C+Ni+Cr (green) samples. Asterisks corresponds to the $\text{Cu}(K\beta)$ (1.39222\AA) and $\text{W}(LA1)$ (1.47639\AA) radiations. For C+Ni+Cr lines supplemental of the $\{(002), (004), (006)\}$ set are detected and plotted in dark green. The x-ray source is copper.

Figure 3: Magnification of the diffraction feature in the 40° - 47° region to show the existence of both hexagonal and rhombohedral boron nitride stackings. The structure at 44.5° is due to a residual of the Ni+Cr flux as well as a second one (not shown) at 51.8° . The x-ray source is copper.

Figure 4: The 8K macro PL spectra in the 5 eV to 6.1 eV range of several samples showing the phonon-assisted transitions typical of hBN (blue spectrum), mixed with the undulations linked to rBN inclusions overlapping with impurities (green and red spectra) as well as signature of the direct bandgap of bBN, dX_b at 6.032 eV. We tentatively identify the 5.72 eV band in C+Ni+Cr as the un-resolved analogue of the iX_h -($LO_T + TO_T$). Dashed orange lines are guides for the eyes.

Figure 5: Enlarged view of the 8K macro PL spectra in the 5.7eV to 6.1 eV range that reveals the signature of the direct bandgap of bBN dX_b at 6.032 eV as well as its 200 meV phonon-assisted replica (green and red spectra). In blue the macro PL of a high purity hBN crystal. Transitions are labelled according to the convention in the literature. State T sits at the middle of the ΓK direction in the Brillouin zone of hBN.

TABLE 1

Table 1 : 2θ powder diffraction values of boron nitride polytypes and their corresponding diffracting planes. The hexagonal (AA') and Bernal phases (AB) share the same 2θ angles. The indices of the rhombohedral (ABC) phase are given in the hkl hexagonal notation, in consistency with the other stackings. The x-ray source is copper.

2θ (deg.)	AA	AA'/AB	ABC
26.77	001	002	003
41.65	100	100	-
42.66	-	-	101
43.91	-	101	-
45.60	-	-	102
50.20	101	102	-
55.15	002	004	006
56.17	-	-	104
59.59	-	103	-
63.28	-	-	105
71.42	102	104	-
76.01	210	210	110
80.57	-	-	107
82.27	211	212	113
85.55	-	105	-
87.96	003	006	009

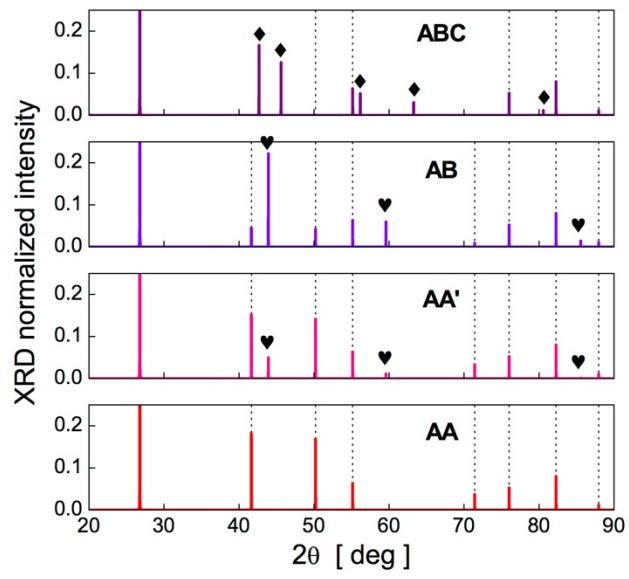


Figure1

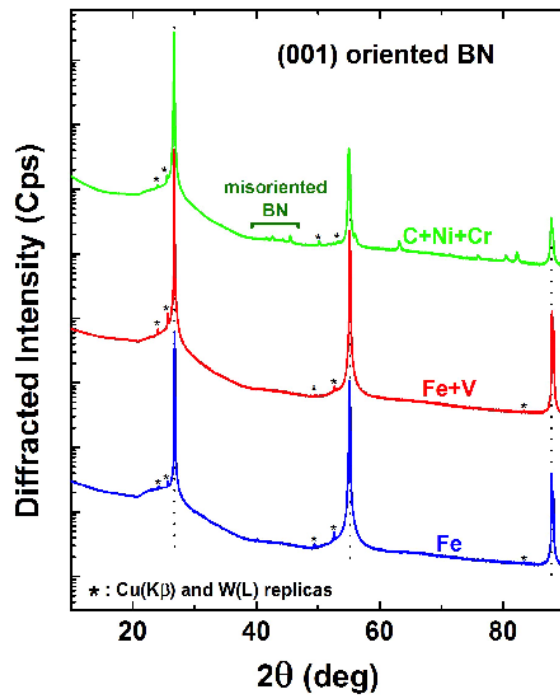


Figure2

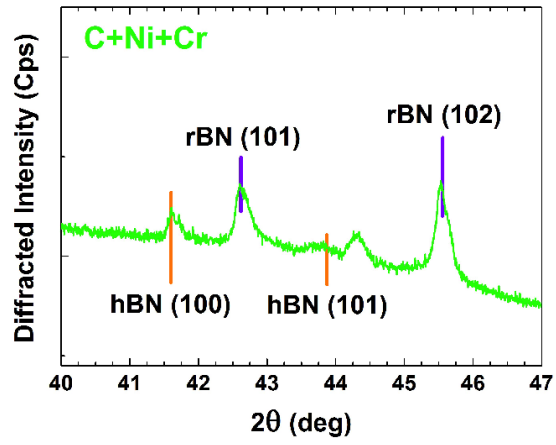


Figure 3

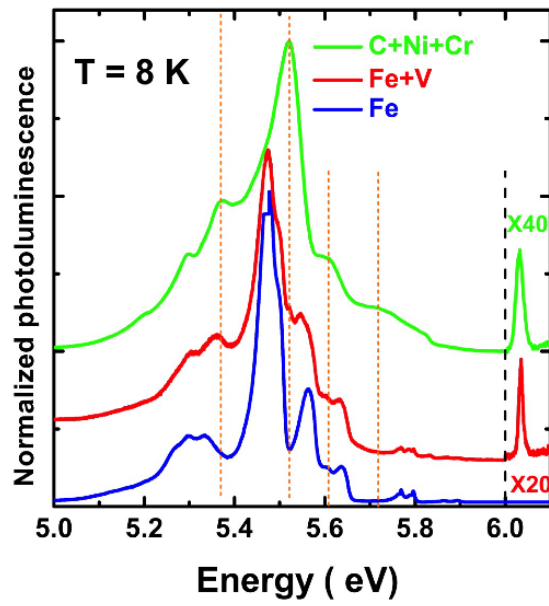


Figure 4

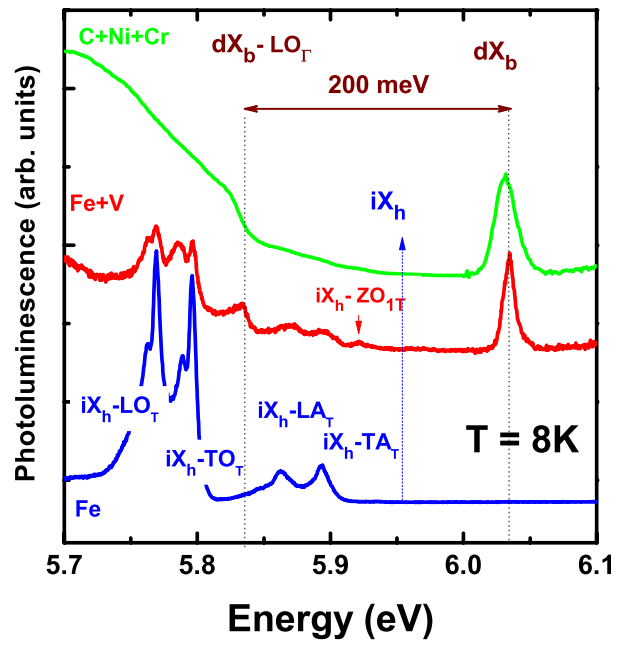


Figure 5